J Mater Sci (2007) 42:6388–6399
DOI 10.1007/s10853-006-1255-5

Atmospheric pressure chemical vapor deposition of transparent conducting films of fluorine doped zinc oxide and their application to amorphous silicon solar cells

Haifan Liang · Roy G. Gordon

Received: 3 August 2006 / Accepted: 10 November 2006 / Published online: 25 April 2007

Abstract Transparent conducting ZnO:F was deposited as thin films on soda lime glass substrates by atmospheric pressure chemical vapor deposition (CVD) deposition at substrate temperatures of 480–500 °C. The precursors diethylzinc, tetramethylethylenediamine and benzoyl fluoride were dissolved in xylene. The solution was nebulized ultrasonically and then flash vaporized by a carrier gas of nitrogen preheated to 150 °C. Ethanol was vaporized separately, and these vapors were then mixed to form a homogeneous vapor mixture. Good reproducibility was achieved using this new CVD method. Uniform thicknesses were obtained by moving the heated glass substrates through the deposition zone. The best electrical and optical properties were obtained when the precursor solution was aged for more than a week before use. The films were polycrystalline and highly oriented with the *c*-axis perpendicular to the substrate. The electrical resistivity of the films was as low as 5×10^{-4} Ωcm. The mobility was about 45 cm^2/Vs. The electron concentration was up to $3 \times 10^{20}/cm^3$. The optical absorption of the films was about 3–4% at a sheet resistance of 7 Ω/square. The diffuse transmittance was about 10% at a thickness of 650 nm. Amorphous silicon solar cells were deposited using the textured ZnO:F films as the front electrode. The short circuit current was increased over similar cells made with fluorine doped tin oxide, but the voltages and fill factors were reduced. The voltage was restored by overcoating the ZnO:F with a thin layer of SnO_2:F.

H. Liang
Division of Engineering and Applied Sciences,
Harvard University, Cambridge, USA

Present Address:
H. Liang (✉)
4253 Sora Terrace, Fremont, CA 94555, USA
e-mail: haifan99@netscape.net

R. G. Gordon
Department of Chemistry and Chemical Biology, Harvard University, 12 Oxford Street, Cambridge, MA 023138, USA

Introduction

Zinc oxide is a large band gap semiconductor (3.3 eV) with a hexagonal wurzite structure. As a thin film, zinc oxide has many practical applications, such as in solar cells, liquid crystal flat panel displays, energy efficient windows, gas sensors, surface acoustic wave devices, piezoelectric devices, ultrasonic transducers, etc. [1–3].

Transparent conductors are materials with low electrical resistivity and high transmittance of visible light. Large band gap semiconducting metal oxides such as indium oxide, cadmium oxide, tin oxide and zinc oxide can be doped with impurity atoms to reduce their resistivity while restaining high transparency in the visible spectrum. Zinc oxide has several advantages over the other transparent conducting oxides. Cadmium in all its compounds is toxic and carcinogenic, and organotin precursors are toxic, while zinc compounds are generally non-toxic. Zinc metal is less expensive than tin, indium or cadmium. For solar cell applications, fluorine doped tin oxide currently is the most widely used front electrode, but tin oxide can be reduced in the hydrogen plasma during the silicon deposition process. This results in elemental tin at the silicon interface that can cause optical loss or diffusion, which can lead to degradation in solar cell efficiency. Zinc oxide is more stable

than tin oxide in a plasma reducing environment. Zinc oxide also has a higher optical transmittance than the other transparent conducting oxides. This suggests zinc oxide may lead to higher solar cell efficiency than tin oxide. For applications in making patterns for liquid crystal flat panel displays, zinc oxide has the advantage of easy etching in aqueous acids such as dilute hydrochloric acid. These advantages suggest that zinc oxide should be a technologically important material for transparent conducting applications.

Zinc oxide films have been successfully deposited by chemical vapor deposition (CVD) [4–14], sputtering [15–18], vacuum evaporation [19], spray pyrolysis [20–22] and other thin film deposition techniques. CVD generally has faster growth rates and better uniformity than the other deposition processes. It is more suitable for large-scale commercial applications. Conductive zinc oxide films have been made by adding impurity dopants such as fluorine [23], boron [24], aluminum [25–31], gallium [32–34], and indium [35, 36].

In this paper, we report the atmospheric pressure chemical vapor deposition of ZnO:F films using the tetramethylethylenediamine adduct of diethylzinc, $(C_2H_5)_2Zn(CH_3)_2NCH_2CH_2N(CH_3)_2$, as the zinc source, benzoyl fluoride (C_6H_5COF) as the fluorine dopant, and ethanol (C_2H_5OH) as the oxygen source. We also investigated the structural, electrical and optical properties of the films, and their applicability to amorphous silicon solar cells.

Experimental

Precursors

The commonly used zinc precursors for chemical vapor deposition of zinc oxide include diethylzinc ($Zn(C_2H_5)_2$), dimethylzinc ($Zn(CH_3)_2$), and zinc acetylacetonate ($Zn(C_5H_7O_2)_2$). Both dimethylzinc and diethylzinc are difficult to handle because they burn spontaneously in air (pyrophoric). They are very reactive to oxygen and moisture, making a CVD process subject to disruption by leaks of air. The resulting films are frequently irreproducible and not uniform. Zinc acetylacetonate is a solid and has low solubility in the common solvents. It is difficult to vaporize as a precursor. Films made with zinc acetylacetonate also have relatively low growth rate and high resistivity ($>10^{-3}$ Ωcm).

The tetramethylethylenediamine adduct of diethylzinc (Et_2Zn(TMEDA)) was synthesized by reacting diethylzinc with tetramethylethylenediamine. It is a compound with a chelate amine ligand attached to the diethylzinc. The zinc atom of the chelated precursor molecule is less accessible than in diethylzinc; therefore the chelated precursor is much less reactive to oxygen and moisture, and is not spontaneously flammable. The new CVD process based on the chelated precursor is more controllable and reproducible, and the films are more uniform. Et_2Zn(TMEDA) is a solid that is easily dissolved in organic solvents such as xylene. Variants of the precursor are made by reacting diethylzinc with other amine ligands, such as tetraethylethylenediamine, *N*,*N*′-dimethyl-*N*,*N*′-diethylethylenediamine, *N*,*N*-dimethyl-*N*′,*N*′-diethylethylenediamine, and *N*,*N*,*N*′-dimethyl-*N*′-diethylethylenediamine. The resultant precursors are liquids at room temperature and have reactivity similar to Et_2Zn(TMEDA). Since teramethylethylene-diamine is less expensive than the other amine ligands, we mainly used Et_2Zn(TMEDA) as the zinc precursor.

An important advantage of these chelated diethylzinc precursors is the ability to premix their vapors homogeneously with ethanol vapor as an oxygen source. In our previous work [23–25] with unchelated diethylzinc, the reaction with alcohol was so fast that premixing could not be used. The vapors had to be mixed directly over the substrate from separate inlets. In a CVD process, homogeneously premixed vapors allow a much simpler injector design with a single inlet. Process reproducibility is also much improved with a homogeneous reactant vapor mixture, because the reactivity does not depend on the details of how the reactant vapors mix at the inlet to the reactor. We also tried other alcohols such as isopropanol. The resulted film conductivity was lower and visible absorption was higher than using ethanol.

Benzoyl fluoride was chosen as the fluorine precursor. It is a stable liquid at room temperature. It dissolves in the zinc precursor solution, and it produced fluorine doping even at low concentrations. We found using benzoyl fluoride as the dopant precursor convenient and reliable, although the fluorine-doped precursor solutions have a limited shelf life, as explained in the results section.

We also used other fluorine sources and found them less suitable. Hexafluoropropene is a gas at room temperature and could be used as the dopant source, but it was not an efficient dopant source and required a large quantity. Other gas phase fluorine sources such as hydrogen fluoride inhibited film growth at even low concentrations. Acetyl fluoride has a boiling point of 20 °C, so it is in between a liquid and a gas at room temperature. Various methods were used to introduce the acetyl fluoride, but reproducibility was poor. Introducing acetyl fluoride as a gas from a heated cylinder did not lead to fluorine-doped films. Dissolving the acetyl fluoride in the zinc precursor solution was not reproducible because the very volatile acetyl fluoride escaped easily from the solution.

Experimental procedure

The ZnO films were deposited in a belt furnace made by BTU International. The experimental set up is schematically shown in Fig. 1. The substrate temperature was varied from 450 °C to 525 °C. The injector included a cylindrical shower head with small holes along the side, housed in a cylindrical chamber leading down to a slot 6 mm wide and 124 mm long. It was designed to make uniform films with all the precursors premixed before entering the injector. Et_2Zn(TMEDA) was synthesized by reacting diethylzinc in xylene with tetramethylethylenediamine. Benzoyl fluoride (from Alfa AESAR) was mixed with Et_2Zn(TMEDA) dissolved in equal weight of xylene. The most stable container for precursor storage were poly-fluorocarbon containers(such as Teflon). Glass or polyethylene containers reacted with the precursor and produced residues. Even in the poly-fluorocarbon lined containers, there were gradual chemical changes within the solution, leading to CVD results that depended on the time elapsed since the mixing of the benzoyl fluoride into the solution.

Anhydrous ethanol was obtained from Pharmco. The water content in commercial anhydrous ethanol was determined using the Carl-Fischer titration method to be about 0.04 weight %.

The zinc precursor was pumped from a syringe pump to a SONOTEK ultrasonic nozzle that turned the solution into a fine mist of droplets of about 20–50 micron in diameter. The precursor injection speed varied from 0.2 ml/min to 1.8 ml/min, corresponding to about 0.1 mol% to 1 mol% in the gas stream. Nitrogen carrier gas, preheated to about 150 °C, met the precursor at the ultrasonic nozzle and vaporized the precursor droplets. The nitrogen gas was purified so that the oxygen content was in the parts per billion level. The nitrogen carrier gas flow rate varied from 8 l/min to 12 l/min. Ethanol was introduced through another line, also from a syringe pump. The injection speed varied from 1.0 ml/min to 6.0 ml/min, corresponding to about 3 mol% to 30 mol% in the gas stream. Ethanol was vaporized at a 1/16″ Swagelok tee joint by nitrogen carrier gas heated to 80 °C. The carrier gas flow rate for ethanol was set to 1.6 l/min.

Two types of experiments were carried out. One was a static deposition where the substrates were stationery during the deposition. This was used to study the flow pattern and kinetics of the deposition process. The other type was a moving deposition where the substrates were moved by a belt at a constant speed across the reaction zone so that a uniformly thick film could be deposited. The belt speed varied from 0.5 inch/min to 10 inch/min.

Soda lime glass and silicon were used as the substrates. Soda lime glass was projector slide glass from Kodak. Silicon was 4 inch wafers from Silicon Sense Inc. The substrates were first cleansed with soap and water, then rinsed thoroughly with deionized water, then blown dry with dry air. The substrates were put on a substrate holder

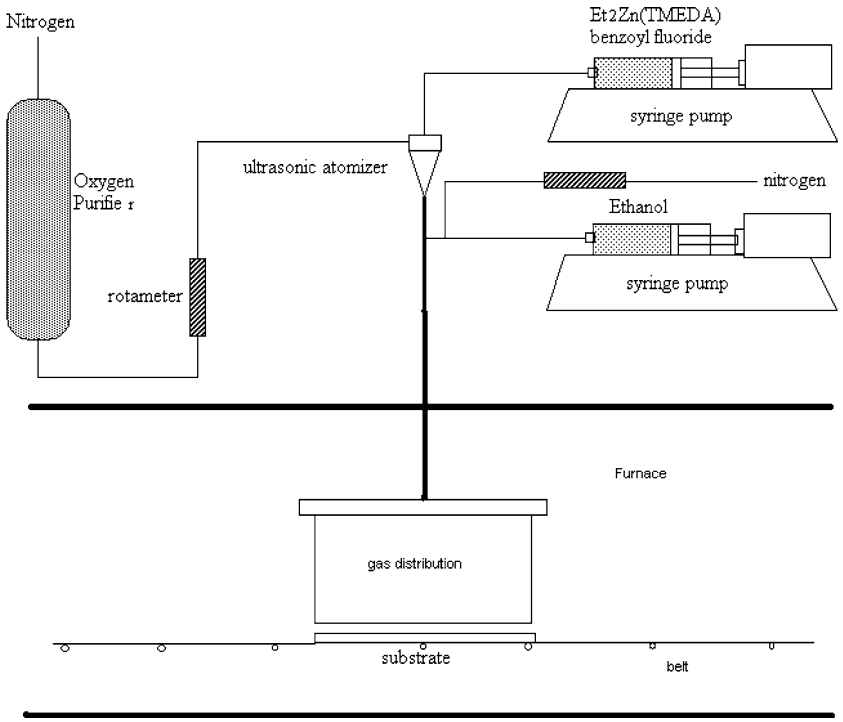

Fig. 1 Schematic drawing of the experimental setup

designed so that the substrate surface was level with the substrate holder surface. This produced a more uniform flow across the substrate surface and minimized edge effects. The substrate holder was made from either stainless steel or aluminum. The substrate surface temperature was profiled by cementing a thin thermocouple on the substrate. The substrate temperature was 30–50 °C below the furnace temperature.

Film thickness was measured with a Tencor Alpha-Step 200 profilometer. A step was generated by covering the film with Scotch tape and etching in 4 M HCl. The sheet resistance was measured with a Veeco FPP-100 four point probe. The mobility and electron concentration of the films were measured using van der Pauw's method.

Optical properties were measured with a Hitachi U-4001 spectrophotometer with an integrating sphere detector. For textured ZnO films on glass, light trapped by total internal reflection causes a higher value of the measured absorption. To correct for this effect, an index fluid of $n = 1.76$ was sandwiched between the film and a thin cover glass during measurement

X-ray diffraction spectra were obtained on a GE X-ray diffraction machine with iron K radiation. The X-ray wavelength was 1.93604 Å. The operating voltage was 40 kV and the current was 10 mA. A manganese filter was used to filter out the iron Kβ line, but a slight amount of Kβ radiation still passed through, as could be seen from the small Kβ line diffraction peaks in the X-ray spectra.

Rutherford backscattering spectra were obtained using a General Ionics Model 4117 spectrometer. The operating He^+ beam energy was 2.0 MeV. Fluorine concentration was measured using electron microprobe analysis (EMA). It was done on a Cameca MBX electron microprobe using wavelength dispersive spectrometers. The operating beam voltage was 5 keV, beam current was 20 nA, and beam size was 32 μm × 32 μm. The standard for calibration was calcium fluoride.

Film morphology and crystallite size were studied with a LEO 982 Scanning Electron Microscope with GEMINI column.

Results and discussion

Film deposition

Static depositions were first made to study the flow pattern and kinetics of the deposition process. On bare soda lime glass, results were not reproducible and sometimes no film was deposited, or film was only deposited on parts of the substrate. This was attributed to the inability of ethanol to react directly with the zinc precursor. A thin layer (a few tens of nm) of Al_2O_3, TiO_2, ZnO or SnO_2 precoated on the glass substrates did initiate reproducible ZnO growth, probably by catalyzing the dehydration of ethanol to water. As ZnO was grown and covered these oxides, its own surface also acted as a catalyst for the dehydration of ethanol to grow a next layer of ZnO on top. The results were reproducible when the substrates were precoated with any one of these oxides of aluminum, titanium, zinc or tin, all of which are known to catalyze the dehydration of alcohols. Alternatively, if a small amount of water vapor was introduced into the reaction zone just before the deposition began, it reacted with the zinc precursor to form a thin layer of ZnO on bare soda lime glass and initiated reproducible film growth.

Because the zinc precursor and ethanol were premixed before entering the injector, and large amount of ethanol was used, it was important to use anhydrous ethanol. Even trace amounts of water in the ethanol (>0.1%) could react with the zinc precursor to form powder before entering the reaction zone. For example, 0.4% water in the ethanol reduced film thickness by 40%. The ethanol to zinc molar ratio was greater than 10. If lower amounts of ethanol were used, the films looked brown in transmission. Both the optical absorption and the film resistivity increased. These effects may be due to carbon incorporation in the films from incomplete reaction of the zinc precursor.

Below a substrate temperature of 450 °C, very little film was grown. At zinc precursor concentration 0.3 mol%, the film growth rate increased with substrate temperature until 480 °C. Above 480 °C the growth rate remained the same. At a higher zinc precursor concentration of 0.9 mol%, the growth rate increased with substrate temperature until 510 °C. Increasing the precursor concentration required a higher substrate temperature to achieve a similar deposition efficiency. The maximum growth rate was as high as 1,000 nm/min near the entrance of the gas flow. The ethanol concentration did not affect the film growth rate over a broad range. The benzoyl fluoride concentration in the precursor affected the growth rate, and its effect depended on how long the precursor mixture was aged after mixing in the benzoyl fluoride. If the precursor solution was not aged, a high benzoyl fluoride concentration (>3 mol%) strongly inhibited film growth. If the precursor was aged for more than one week, the inhibition effect did not occur until a much higher fluorine concentration was reached. The dependence of the growth rate on fluorine concentration for the aged precursors is shown in Fig. 2.

Films made with static deposition usually had the maximum growth rate right under the inlet slot in the injector. As the precursor was gradually depleted, film growth rate became lower near the two exhaust slots. Looking at the film in reflectance showed stripes of interference color bands from the variation in thickness. Moving the substrate through the deposition zone produced

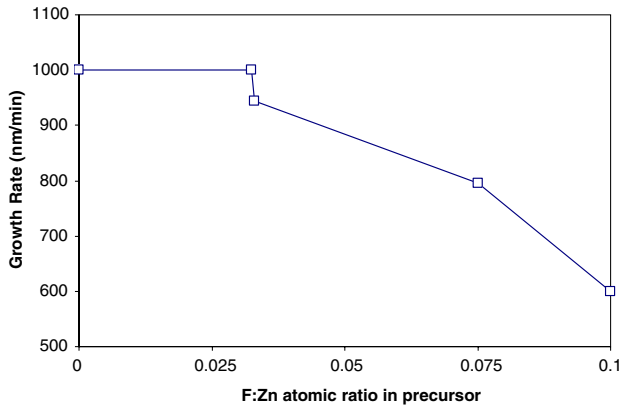

Fig. 2 Dependence of the growth rate on fluorine concentration in the precursor (static deposition, substrate temperature: 495 °C; Et_2Zn(TMEDA):0.6 mol%; Ethanol:12 mol%; N_2:12 l/min)

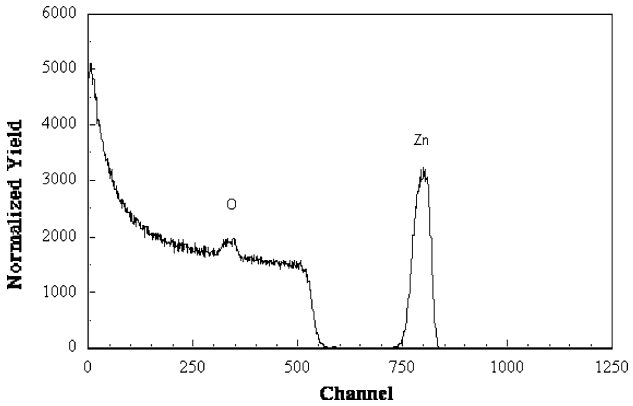

Fig. 3 RBS spectrum of a ZnO:F film (Substrate temperature:495 °C; Et_2Zn(TMEDA):0.6 mol%; F/Zn mol ratio:1/27; Ethanol:12 mol%; N_2:12 l/min; Belt bspeed:2 inch/min)

uniformly thick films over the entire substrate. It was found that a precoating on the soda lime glass substrate was not necessary for uniform film growth during moving depositions. This was attributed to the substrate holder surface next to the substrate, which already had ZnO on top. The ZnO could catalyze the dehydration of ethanol into water and film growth could be initiated on the bare soda lime glass substrate. We confirmed this hypothesis by running depositions on bare soda lime glass substrates without using the substrate holder. The nucleation was poor without the substrate holder, indicating the necessity of an oxide layer to initiate growth. The maximum growth rate for moving deposition was about 240 nm/min.

The deposition efficiency of the reaction for optimal doped films was about 30%.

Composition and crystal structure

Rutherford back scattering (RBS) spectra were obtained for the best electro-optic quality films deposited on silicon. RBS (Fig. 3) spectra showed the zinc oxide films had a Zn:O = 1:1 stoichiometry. No carbon was detected in RBS. Since the fluorine content was very low and the fluorine signal sat on the silicon background, we could not detect the fluorine signal in the RBS spectra. Electron microprobe analysis (EMA) with calcium fluoride as a standard gave fluorine concentration of 0.2–0.3 atomic percent. Since the fluorine concentration was near the detection limit, the results should be taken as only an estimate of the fluorine concentration.

X-ray diffraction patterns of all films grown in this study were crystalline with a hexagonal wurzite structure. Figures 4 and 5 show the X-ray spectra of undoped and fluorine doped ZnO films grown at 495 °C. Besides a small (103) peak in the undoped film, the main peaks were at (002) for both samples, indicating the crystallites had a

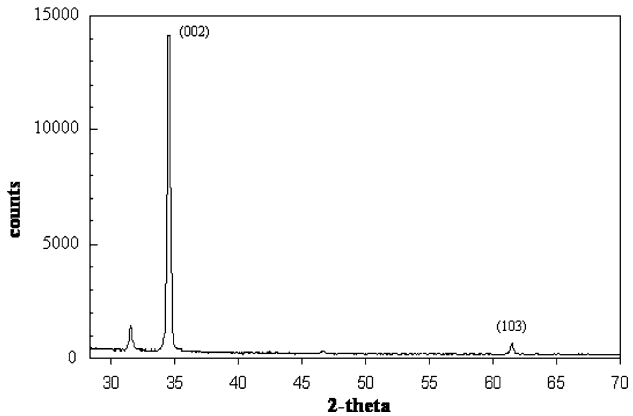

Fig. 4 X-ray spectrum of undoped ZnO (deposition temperature 495 °C), X-ray source: Mn-filtered Fe K lines

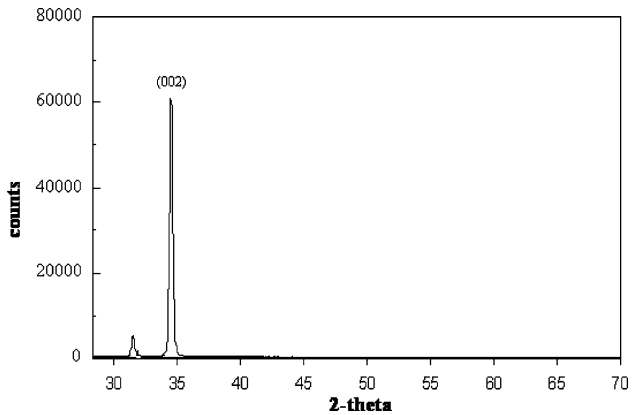

Fig. 5 X-ray spectrum of ZnO:F (deposition temperature 495 °C, X-ray source: Mn-filtered Fe K lines

strong orientation with the c-axis perpendicular to the substrate. The peaks near $2\theta = 32°$ were from iron Kβ radiation in the X-ray source. The lattice constant of

undoped zinc oxide was c = 5.193 Å, closely matching the published value c = 5.207 Å [37]. The fluorine doped film had a very slight shift of $\Delta(2\theta) = 0.02°$ of the (002) peak towards the lower angles, corresponding to a small increase in the bond length. The n-type doping placed electrons in the anti-bonding conduction band, thereby weakening and lengthening the bonds.

The full width at half maximum of the (002) peaks of both the undoped and fluorine doped ZnO films were the same. This indicated the crystallite sizes along the c-axis for both films were the same. An estimate of the crystallite size in the direction perpendicular to the substrate was calculated using the Scherrer equation [38]:

$$t = 0.9\lambda/\beta\cos\theta \quad (1)$$

where λ is the wavelength of the X-ray, θ is the angular diffraction peak position, and β is the FWHM of the peak. The calculated crystallite thickness was about 30 nm for a film 0.8 micron thick.

Electrical properties

Film resistivity was measured from the sheet resistance and the film thickness. The films deposited using moving substrates had good uniformity in both the film thickness and sheet resistance, usually with a variation of less than 10% over the entire substrate area. Variation mainly occurred near the edges. The edge area usually had slightly higher sheet resistance and lower growth rate. This could come from a small variation of the temperature over the substrate. Deposition parameters such as the substrate temperature, dopant concentration, precursor aging time, and ethanol concentration were varied to optimize the film resistivity.

The mobility of thin films generally increased with the substrate temperature. The optimum substrate temperature was around 480–500 °C. At substrate temperatures above 500 °C, the mobility and the electron concentration started to decrease. Possible explanations are either the dopant was more difficult to incorporate into the film or the dopant was not as electrically active at the higher temperatures. The dependence of the film thickness and the electrical properties on substrate temperature is shown in Fig. 6.

The aging time of the fluorine and zinc precursors affected the film resistivity. Benzoyl fluoride was premixed with Et_2Zn(TMEDA) in xylene solution and stored in a glove box for up to 2 months. Films made with the precursor aged for more than 1 week, but less than 5 weeks had film resistivity about 30% lower than the films made with precursor aged for less than 1 week. This was probably because the fluorine exchanged with the ethyl group and attached to the zinc atom, resulting in more efficient

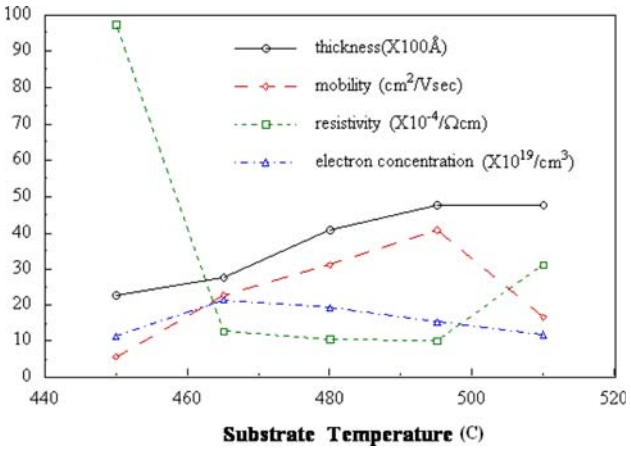

Fig. 6 Electrical properties of ZnO:F films as a function of substrate temperature

doping during film deposition. However, aging the precursor for more than five weeks resulted in higher film resistivity. It was found that both the electron concentration and mobility were lower. This could be due to the formation of zinc fluoride in the precursor or in the film. NMR spectra showed there was a reaction between the zinc and the fluorine precursors over time, but the precise mechanism is not clear.

If the precursor solution was used less than a week after adding the benzoyl fluoride, the film resistivity was very sensitive to the precise concentration of fluorine in the precursor. Even a few percent change in the fluorine concentration resulted in large change of the resistivity. The results were difficult to reproduce. For precursor solutions aged more than a week, the resistivity was much less sensitive to the fluorine concentration in the precursor, and the optimum fluorine concentration had a wider range. The optimum molar ratio of fluorine to zinc was in the range 1:20 to 1:30. The deposition process was more controllable and reproducible when the precursor was aged for a week or more before use. The dependence of the electrical properties on fluorine concentration in the precursor solution is shown in Figs. 7–9.

Ethanol concentration also affected the film resistivity. When ethanol concentration was low (below 10:1 ethanol to zinc molar ratio), the films had higher resistivity. This was probably due to carbon contamination in the film from the incomplete decomposition of the zinc precursor. The resistivity was optimized over a relatively wide range of ethanol concentration. The optimum molar ratio of zinc to ethanol was about 1 to 20. When the ethanol concentration was too high, the resistivity increased. The increase in resistivity mainly came from a decrease in the carrier concentration, indicating doping was less efficient when the ethanol concentration was high.

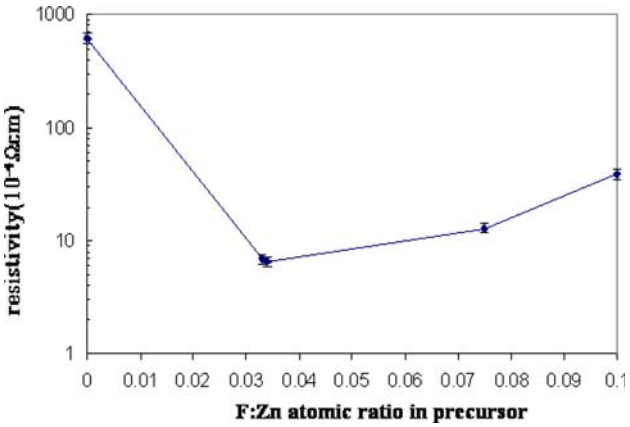

Fig. 7 Dependence of the resistivity of ZnO:F on the fluorine concentration in the precursor

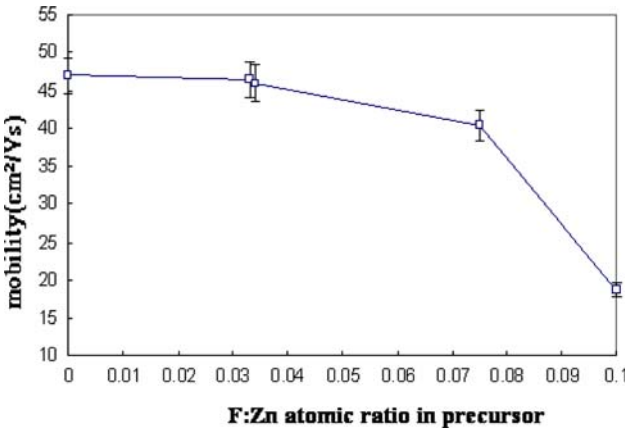

Fig. 8 Dependence of the mobility of ZnO:F on the fluorine concentration in the precursor

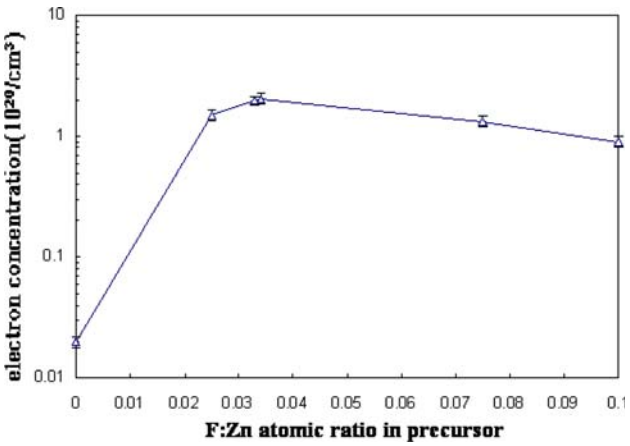

Fig. 9 Dependence of electron concentration of ZnO:F films on the F concentration in the precursor

The resistivity depended on the film thickness. Thinner films had higher resistivity. Generally, the mobility of thinner films was lower because of the smaller grain size. This resulted in larger grain boundary scattering of the free electrons. We found that both the mobility and electron concentration were lower for thinner ZnO:F films. The decrease in electron concentration could be attributed to the increase of trapping states at the grain boundaries when the grain sizes were smaller. Figure 10 shows the dependence of the resistivity on film thickness. The thickness of these films was varied by changing the speed at which the substrate moved across the reaction zone. For films with thickness less than 300 nm, film resistivity depended very strongly on the film thickness, since grain boundary scattering was important for thinner films with small crystallite sizes. For films with thickness greater than 300 nm, film resistivity depended only weakly on the film thickness. Grain boundary scattering was less important when the crystallite sizes were large. The mobility of the thicker films was dominated by ionized impurity scattering. For amorphous solar cell applications, we wanted films with low sheet resistance (<15 Ω/square) and a high diffuse transmittance (>10% near 650 nm); both of these qualities required thick films. We concentrated on investigating films with thickness in the range of 700–900 nm.

The electrical properties of undoped and fluorine doped zinc oxide films were measured for comparison. The only difference in deposition condition was the benzoyl fluoride in the precursor. The optimized fluorine to zinc molar ratio in the precursor was 1:27. The substrate temperature was 495 °C. The zinc precursor concentration was 0.6 mol% in the gas phase. The ethanol vapor concentration was 12 mol%. The total carrier gas flow was 12 l/min. The exhaust flow was 24 l/min. The belt speed was 2 inch/min. Both the undoped and doped films had similar mobility of

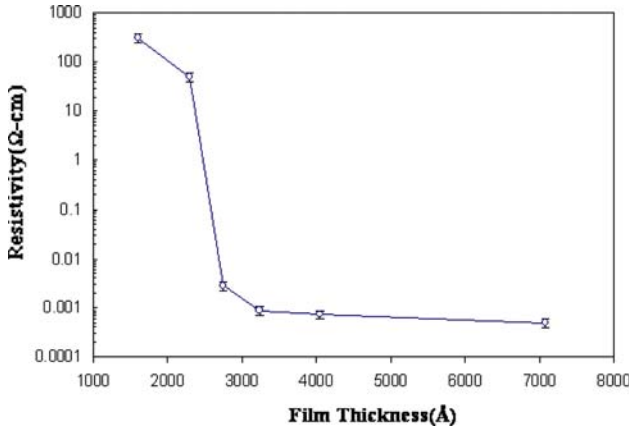

Fig. 10 ZnO:F films resistivity versus thickness (Substrate temperature:495 °C; Et_2Zn(TMEDA):0.6 mol%; F/Zn mol ratio:1/27; Ethanol:12 mol%; N_2:12 l/min; Belt speed:1–10 inch/min)

about 45 cm^2/Vs. This was higher than other transparent conductors such as indium tin oxide and fluorine doped tin oxide. Doping increased the electron concentration by two orders of magnitude. The undoped films had electron concentration of the order of $10^{18}/cm^3$, and the fluorine doped films had electron concentration of around $2 \times 10^{20}/cm^3$. The film resistivity of the ZnO:F films was as low as 5×10^{-4} Ωcm.

Fluorine was expected to replace oxygen in the zinc oxide lattice and contribute free electrons, but they also acted as ionized impurity scattering centers. SEM micrographs (Fig. 11) showed that when the fluorine concentration in the precursor was high, the grain size decreased. Grain boundary scattering increased when the grain size decreased. Therefore, the mobility of films with high fluorine concentration decreased due to both the increase in ionized impurity scattering and grain boundary scattering. A high fluorine concentration in the films did not necessarily lead to a higher electron concentration. The fluorine atoms needed to replace the oxygen atoms in the zinc oxide crystal structure if they were to contribute free electrons. If the fluorine atoms did not occupy the proper oxygen sites or if they formed zinc fluoride, they would not provide free electrons and could change the morphology and grain size of the films. The SEM micrographs (Fig. 11) showed the undoped films had large grain size with a hexagonal structure. The crystallites were plate-like and thin in one of the dimensions. The plates were randomly tilted, indicating the crystallites were not completely oriented with the *c*-axis perpendicular to the substrate surface. Fluorine doped films with the optimum fluorine concentration for low resistivity had a hexagonal columnar structure. The crystallites were thick and shrinked near the top. The columns were highly oriented with the *c*-axis perpendicular to the substrate surface. The optimal doped films were more oriented than the undoped films. Films with higher than optimum fluorine content had a plate-like morphology similar to the undoped films but with smaller crystallite sizes.

Optical properties

Transmission and reflection spectra were taken to study the optical properties of the films. The total transmittance and reflectance of a ZnO film with optimum fluorine doping is shown in Fig. 12. The film thickness was about 800 nm and the sheet resistance was about 7 Ω/square. Optical absorption and texture were the two main optical properties we tried to optimize. For solar cell applications, a low optical absorption is desired to allow more photons to enter the active cell region and generate electron-hole pairs. Film texture is desired to provide light trapping in the cell in order to lengthen the light path in the cell. This is

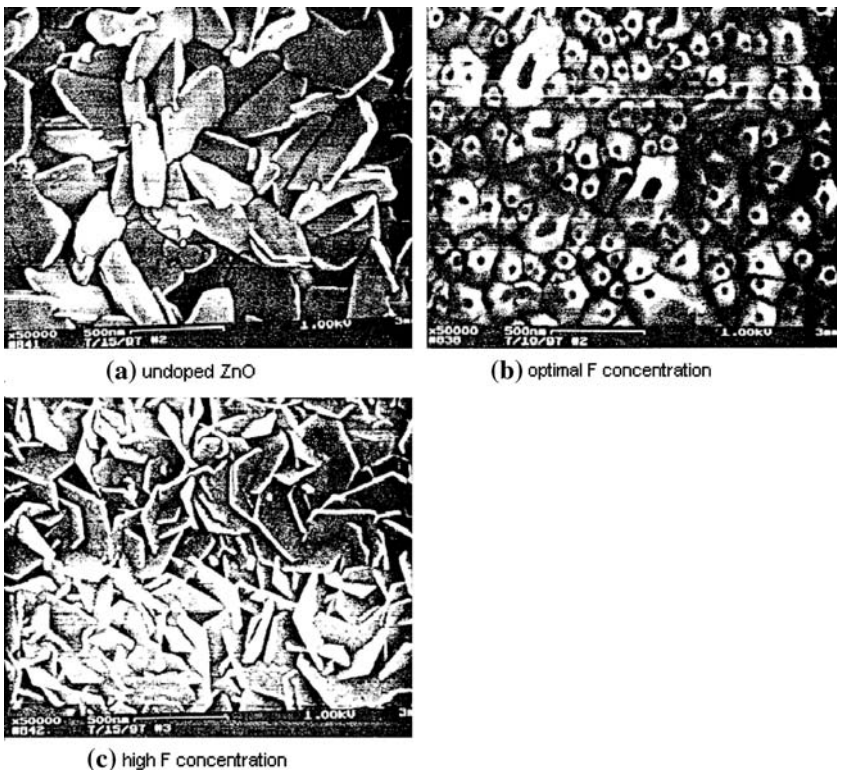

Fig. 11 SEM micrographs of ZnO films (**a**) undoped, (**b**) optimal F concentration, (**c**) high F concentration

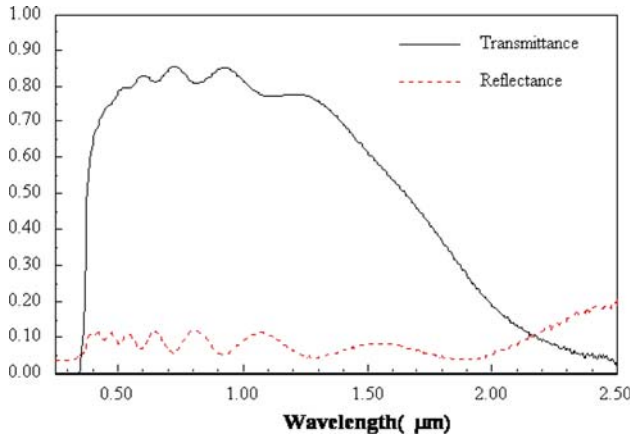

Fig. 12 Total transmittance and reflectance spectra of a ZnO:F film. (Sheet resistance: 7 Ω/square, thickness 8,000 angstroms)

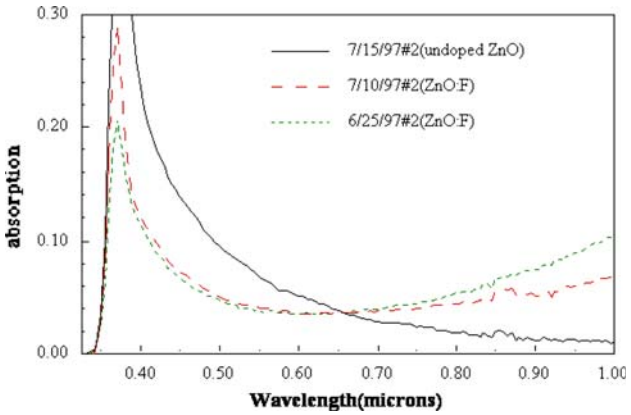

Fig. 13 Optical absorption of undoped and fluorine doped ZnO films(Substrate temperature:495 °C; Et_2Zn(TMEDA):0.6 mol%; F/Zn mol ratio:0 to 1/27; Ethanol:12 mol%; N_2:12 l/min; Belt speed:2 inch/min)

especially important for silicon in the near infrared region of the spectrum, since silicon does not absorb strongly in this region.

Deposition conditions such as the substrate temperature, dopant concentration, and ethanol concentration were varied to study the optical absorption of the films. Film absorption was mainly affected by the ethanol concentration. Low ethanol concentration resulted in a brown film with large absorption. This was attributed to carbon contamination due to the incomplete decomposition of the zinc precursor. Optical absorption decreased with increasing ethanol concentration. This had to be compromised with electrical resistivity, since a higher than optimum ethanol concentration increased the film resistivity.

Doping the films with fluorine generated free electrons, which modified the optical properties of the films. Increasing the electron concentration in the film also led to increased absorption in the visible region from free electron absorption. The absorption coefficient α in the visible region is given by [39]:

$$\alpha = 4\pi k/\lambda = (e^3/4\pi^2 \varepsilon_0 c_o^3)\lambda^2 n_e / m^{*^2} \mu n) \quad (2)$$

where n and k are the real and imaginary parts of the refractive index, λ is the wavelength, n_e is the free electron concentration, m^* is the effective mass, and μ is the mobility. Since the fluorine doped zinc oxide films had high mobility and low electron concentration, film absorption was lower than other transparent conductors such as indium tin oxide and fluorine doped tin oxide. The solar weighted average absorption in the wavelength region 400–700 nm was as low as 3–4% for films with a sheet resistance about 7–8 Ω/square.

Figure 13 shows the absorption spectra of undoped and doped zinc oxide films. The doped zinc oxide film showed increased absorption in the near infrared region due to the increase in free electron concentration. The doped zinc oxide films had lower absorption in the near ultra-violet region because of the Moss-Burstein effect. The Moss-Burstein effect is partly offset by a band gap narrowing effect due to carrier-carrier interactions and carrier-impurity interactions. For heavily doped films such as the ZnO:F, the Moss-Burstein effect is dominant and the absorption edge shifted to the lower wavelengths. This effect is advantageous in solar cell applications to allow more photons in the near ultra-violet region to enter the cell. It can also be useful in some optoelectronic devices where band gap tailoring is required.

Film texture was measured by the diffuse transmittance of the films. For effective light trapping, about 5% diffuse transmittance at 650 nm is adequate to enhance cell performance [40]. We found that the film texture depended on the substrate temperature, ethanol concentration, and dopant level. Texture increased with the substrate temperature. This was due to the increase in grain size at the higher temperatures. Texture decreased when the ethanol concentration was high. The nucleation density was probably higher when the ethanol concentration was high, leading to smaller crystallite sizes and smoother films. Texture also decreased with increasing fluorine dopant concentration. Figure 14 shows the diffuse transmittance spectra of undoped, optimally doped and highly doped films. For the optimal doped films, more than 10% diffuse transmittance was achieved at 650 nm.

Thermal stability

The electrical and optical properties ZnO:F films were stable at room temperature. The thermal stability of the films was studied by annealing the films at 400–500 °C in the furnace for half an hour (Table 1). The furnace was

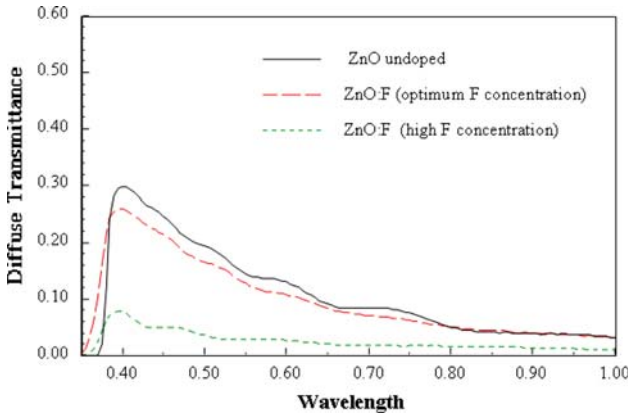

Fig. 14 Diffuse transmittance spectra of undoped and F doped ZnO films (Substrate temperature: 495 °C; Et_2Zn(TMEDA):0.6 mol%; F/Zn mol ratio:0 to 1/9; Ethanol:12 mol%; $N_2$2:12 l/min; Belt speed:2 inch/min)

filled with large flows of nitrogen, but oxygen could not be complete eliminated due to the open construction of the furnace. At 400 °C, the resistivity was relatively unchanged after annealing. At higher temperatures, the resistivity increased after annealing. The percent increase in resistivity was higher at the higher annealing temperatures. At 500 °C, the resistivity was increased by at least an order of magnitude. Some of the free electrons in the film could be contributed by oxygen vacancies. Annealing in an oxygen containing environment caused oxygen to enter the film and filled some of the oxygen vacancies. This could reduce the carrier concentration and increase the resistivity. At high annealing temperatures, oxidation was more efficient and there could be sodium diffusion from the soda lime glass substrate. Sodium in the film could increase defect scattering and lower the mobility. This could also increase the resistivity. The increase in resistivity was higher for more resistive films. Films with lower resistivity had more fluorine in the film. The fluorine atoms replaced the oxygen sites. Therefore there were fewer oxygen vacancies in the more conductive films and they were more stable under annealing. Films with higher resistivity had less fluorine and more oxygen vacancies. Their resistivity increased more rapidly when the oxygen vacancies were filled by the ambient oxygen during annealing.

Films were also annealed in 10% oxygen and 90% nitrogen at 400 °C to study their stability in an oxygen environment. These films were annealed for about 10 min to simulate the deposition of another layer on the film. The resistivity did not change for films with resistivity less than 8×10^{-4} Ωcm. The resistivity increased for films with higher resistivity. The percent increase in resistivity was higher when the film resistivity was higher.

Application to amorphous silicon solar cells

The applicability of ZnO:F as a front electrode on a:Si cells were tested at Solarex and University of Delaware. The structure of the cells is shown in Fig. 15. Both groups reported an increase of about 5% in the short circuit current using ZnO:F compared to the standard SnO_2:F films, This is consistent with the higher transparency of the ZnO than the SnO_2. The open circuit voltages of the cells made on ZnO:F were, from 10 mV to 100 mV lower than control cells on SnO_2. This can be explained by the lower work function of ZnO compared to SnO_2 [41]. The fill factors of ZnO:F cells were also lower, by 3–10%, than cells made on SnO_2:F. This is attributed to the higher contact resistivity of ZnO/Si than SnO_2/Si. Both the lower work function and the lower electron concentration contributed to the increase in contact resistivity when using ZnO:F.

To resolve the voltage and contact resistivity problems of ZnO, a thin layer (a few hundred angstroms) of heavily doped SnO_2 was deposited between the ZnO and the p-type a:Si layer. The SnO_2 layer should be thin enough to retain high light transmission, but thick enough to provide good electrical contact. The structure SnO_2:F/thick ZnO:F/glass should combine the best features of the two materials for a:Si solar cells. The thick ZnO:F should provide high transparency, and the thin SnO_2:F should provide good electrical contact to the silicon.

Table 1 Sheet resistance change of ZnO:F films annealed in one atmosphere of nitrogen gas for 30 min at various temperatures

F:ZnO film	Original sheet resistance (Ω/square)	Sheet resistance after annealing for 30 min				
		400 °C	425 °C	450 °C	475 °C	500 °C
Sample #1	10.1	10.1	12.0	13.9	29.4	527
Sample #2	12.9	13.6	18.9	21.7	51.0	1,900
Sample #3	13.6	14.6	22.4	27.8	76.4	6,600

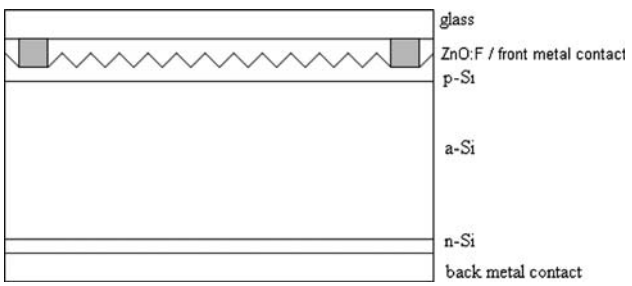

Fig. 15 Structure of an amorphous silicon solar cell with textured ZnO:F front electrode

The standard CVD deposition temperature of SnO_2:F is above 500 °C. This would lead to an increase of sheet resistance in the underlying ZnO:F film. We investigated the deposition of SnO_2:F at lower temperature, and found SnO_2:F could be deposited at 460 °C by the reaction of tetramethyltin, oxygen and hexafluoropropene. The free electron concentration in the SnO_2:F was 5×10^{19} cm^{-3}, an order of magnitude lower than the values usually found for optimized SnO_2:F deposited at higher temperatures.

Amorphous silicon solar cells were deposited on samples of the thin SnO_2:F/thick ZnO:F/glass transparent conductors using three different boron dopant levels in the p-Si layer. The lowest flow is typical of was used for standard SnO_2 substrates. Figure 16 shows that the standard boron doping level gave lower open-circuit voltages on the ZnO substrate than on SnO_2. The thin, lightly doped SnO_2 layer on the composite SnO_2:F/ZnO:F raised the voltage back to the level found in the same run for standard SnO_2. This result supports the potential of the composite SnO_2:F/ZnO:F to increase cell efficiency.

At the higher levels of boron doping, the voltages became equivalent for all of the substrates. The fill factors increased with boron doping level, but, unfortunately, remained lower for both ZnO-containing substrates, at all boron doping levels (Fig. 17). Apparently, a higher free electron concentration will be needed in the tin oxide contact layer, if higher fill factors and efficiencies are to be attained with the composite SnO_2:F/ZnO:F transparent conductor.

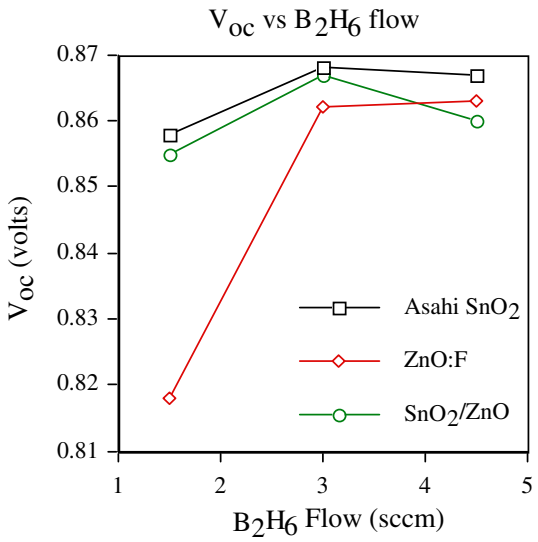

Fig. 16 Open circuit voltages for amorphous silicon solar cells grown on three different transparent conductors, as a function of the boron doping level in the p-layer

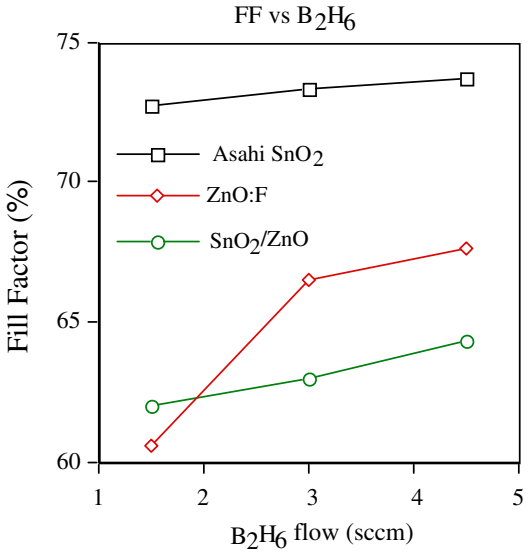

Fig. 17 Fill factors for amorphous silicon solar cells grown on three different transparent conductors, as a function of the boron doping level in the p-layer

Summary

We successfully deposited highly transparent conducting textured ZnO:F films from Et_2Zn(TMEDA), ethanol, and benzoyl fluoride. The new precursor and injector design produced uniform films with good reproducibility. A catalytic oxide was needed to dehydrate the ethanol and start film growth on bare glass substrates. The film growth rate increased with precursor concentration, but the deposition efficiency became lower. The growth rate decreased with fluorine dopant concentration. The films were polycrystalline and highly oriented with the *c*-axis perpendicular to the substrate. The crystallites were pointed columnar with diameters between 100 nm and 500 nm and height of about 28 nm. The resistivity decreased with the film thickness. The aging time of the zinc and fluorine precursor solution affected the electrical and optical properties of the films. The mobility decreased with dopant concentration and was optimized at about 480–500 °C. The mobility was about 45 cm^2/Vs. The electron concentration increased with dopant concentration and decreased after a maximum was reached. The electron concentration was up to $3 \times 10^{20}/cm^3$. The resistivity was as low as 5×10^{-4} Ωcm. Film absorption decreased with increasing ethanol concentration, but the conductivity and the texture of the films decreased when the ethanol concentration was too high. The optimum zinc to ethanol molar ratio was about 1:20. Visible absorption was only 3–4% at a sheet resistance of 7 Ω/square. The diffuse transmittance can be varied from about 1–10% at 6,500 Å. We conclude the excellent electrical and optical properties of the ZnO:F films, together with

good uniformity and reproducibility, makes it an attractive candidate for many applications as a transparent conductor. Application to more efficient amorphous silicon solar cells will require a thin contact layer of highly doped tin oxide.

Acknowledgements This work was supported by the National Renewable Energy Laboratory. Steven Hegedus (Delaware) and David Carlson (Solarex) deposited and characterized the amorphous silicon solar cells. John Thornton, Keith Kramer, Dan Teff and Nicholas DiCeglie provided assistance in the chemical preparations and analyses. The authors would also like to thank Yuan Z. Lu, David Lange, and John Chervinsky for their assistance in making some of the characterization measurements.

References

1. Hickernell FS (1976) Proc IEEE 64:631
2. Dutta S, Jackson HE, Boyd JT, Hickernell FS, Davis RL (1981) Appl Phys Lett 39:206
3. Igasaki Y, Saito H (1991) J Appl Phys 70:3613
4. Adachi K, Sato K, Gotoh Y, Nishimura H (1991) Proc of 22nd IEEE PVSC
5. Adachi K, Sato K, Gotoh Y, Nishimura H (1991) Proc of 22nd IEEE PVSC
6. Shiosaki T, Yamamoto T, Yagi M, Kawabata A (1981) Appl Phys Lett 39:399
7. Shiosaki T (1978) Proc IEEE Ultrasonics Symp 100
8. Shiosaki T, Ohnishi S, Kawabata A (1979) J Appl Phys 50:3113
9. Oda S, Tokunaga H, Kitajima N, Hanna J, Shimizu I, Kokado H (1985) Jap J Appl Phys 24:1607
10. Smith FTJ (1983) Appl Phys Lett 43:1108
11. Kim JS, Marzouk HA, Reucroft PJ, Harmin CE (1992) Thin Solid Films 217:133
12. Shimizu M, Katayama T, Shiosaki T, Kawabata A (1990) J Cryst Growth 101:171
13. Wieldraaijer W, van Balen Blanken J, Kupiers EW (1993) J Cryst Growth 126:305
14. Souletie P, Bethke S, Wessels BW, Pan H (1988) J Cryst Growth 86:248
15. Webb JW, Williams DW, Buchanan M (1981) Appl Phys Lett 39:640
16. Minami T, Nanto H, Takata S (1982) Appl Phys Lett 41:958
17. Exarhos GJ, Sharma SK (1995) Thin Solid Films 270:27
18. Jacobsohn E, Shehtman D (1992) Mat Res Soc Symp Proc 242:779
19. Brody DE, R Singh, Morgan JH, Lesli JD, Moore CJ, and A Dixon (1980) In: Proceedings of the 12th IEEE Photovoltaic Specialist Conference. IEEE, New York
20. Kruncks M, Mellikov E (1995) Thin Solid Films 270:33
21. Major S, Banergee A, Chopra KL (1986) J Mater Res 1:300
22. Aranovich J, Ortiz A, Bube RH (1979) J Vac Sci Technol 16:9
23. Hu J, Gordon RG (1991) Solar Cells 30:437
24. Hu J, Gordon RG (1992) J Appl Phys 71:880
25. Hu J, Gordon RG (1992) J Electrochem Soc 139:2014
26. Sato H, Minami T, Miyata T, Ishii M (1994) Thin Solid Films 246:65
27. Minami T, Sato H, Imamoto H, Takata S (1992) Jpn J Appl Phys 31:L257; Minami T, Sato H, Sonohara H, Takata S, Miyata T, Fukuda I (1994) Thin Solid Films 253:14
28. Jin ZC, Hamberg I, Granqivst CG (1988) J Appl Phys 64:5117
29. Aktaruzzman AF, Sharma GL, Malhotra LK (1991) Thin Solid Films 198:67
30. Nishino J, S Ohshio, Kamata K (1992) J Am Ceram Soc 75:3469
31. Tominaga K, Kataoka M, Ueda T, Chong M, Shintani Y, Mori I (1994) Thin Solid Films 253:9
32. Hu J, Gordon RG (1992) J Appl Phys 72:5381
33. Hirata GA, McKittric J, Cheeks T, Siqueiros JM, Diaz JA, Contreras O, Lopez OA (1996) Thin Solid Films 288:29
34. Wang R, King LLH, Sleight A (1996) J Mater Res 11:1659
35. Hu J, Gordon RG (1991) Mat Res Soc Symp Proc 283:891
36. Olvera ML, Maldonado A, Asomoza R, Konagai M, Asomoza M (1993) Thin Solid Films 229:196
37. Dana's System of Mineralogy, 7th Ed I 504
38. Nuffield EW (1966) X-ray diffraction methods. John Wiley & Sons, New York
39. Chopra KL, Major S, Pandya DK (1983) Thin Solid Films 102:1
40. Gordon RG, Proscia J, Ellis FB, Delahoy AE (1989) Solar Energy Mater 18:263
41. Ahmad Nuruddin, PhD Thesis, University of Illinois, 1997; Ahmad Nuruddin and John Abelson, unpublished results